Int. J. Heat Mass Transfer. Vol. 25, No. 11, pp. 1689–1699, 1982
Printed in Great Britain

0017-9310/82/111689-11 $03.00/0
Pergamon Press Ltd.

AXISYMMETRIC FREE CONVECTION AT SMALL RAYLEIGH NUMBER IN POROUS CAVITIES

J. R. PHILIP
CSIRO Division of Environmental Mechanics, Canberra, A.C.T. 2601, Australia

(*Received* 31 *December* 1981)

Abstract—Various exact solutions are found for axisymmetric small Rayleigh number (R) convection in porous cavities due to a steady radial temperature gradient normal to the gravitational field. Detailed results are presented for cylindrical and toroidal cavities with aspect ratio (λ) arbitrary. The critical R for applicability of the analysis is $O(\lambda^{3/2})$ at large λ, $O(1)$ in $0.1 \leqslant \lambda \leqslant 1$, and at small λ is $O(\lambda^{-1/2})$ for toroids and $O(\lambda^{-1/2}[-\ln\lambda]^{-1})$ for cylinders. The exact solutions for toroids offer insight into the toroidal roll characteristic of axisymmetric convection at small R.

For cylinders (and also for 2-dim. convection at small R in rectangles) a core flow with boundary layers occurs both as $\lambda \to 0$ and as $\lambda \to \infty$. On the other hand, the flow pattern in toroids (and also in ellipses) is invariant, free of cores and boundary layers.

Close analogies between axisymmetric and 2-dim. convection at small R hold also for properties such as the variation with λ of the strength of convection and of the critical value of R.

NOMENCLATURE

A, radial cross-sectional area of axisymmetrical porous cavity;
A_n, coefficients in equations (3.8) and (3.27);
a, length of horizontal (radial) axis of radial cross-section of cavity;
B_n, coefficients in equation (3.8);
b, length of vertical axis of radial cross-section of cavity;
C_n, coefficients in equation (3.12);
c_n, constants defined by equation (3.6);
c, volumetric heat capacity of porous medium;
E^2, parameter of secondary logarithmic oval;
f, function defined by equation (3.2);
g, gravitational acceleration;
H, total convective heat transport across the horizontal mid-plane of the cavity;
h, function defined by equation (3.21);
I_1, modified Bessel function of the first kind of order one;
$\mathcal{I}_n$, integrals defined by equation (3.31);
J_1, J_2, Bessel functions of the first kind of orders one and two;
j_n, nth positive zero of J_1;
K, total radial conductive heat transport within cavity (for toroidal cavity, maximum value of this quantity);
K_1, modified Bessel function of the second kind of order one;
k, permeability of the porous medium;
L, characteristic macroscopic length of the system;
n, integer;
$O(x)$, of order x;
Q, steady radial heat flux per unit axial length;
R, Rayleigh number;
R_1, maximum Rayleigh number for applicability of small R analysis;
r, z, dimensionless forms of r_*, z_*;
r_1, value of r at which $\Psi = \Psi_{max}$ in cylindrical cavities;
r_*, z_*, cylindrical space co-ordinates for axisymmetric systems, with z_* vertical, positive upwards;
r_{*1}, reference radius;
r_{*0}, internal radius of toroidal cavity;
T, dimensionless form of T_*;
T_*, temperature;
ΔT_*, characteristic macroscopic horizontal temperature difference of the system;
u, w, dimensionless forms of u_*, w_*;
u_*, w_*, components of flow velocity in the r_*, z_* directions;
v, dummy variable in equation (3.31);
Y_n, functions of r in equations (3.5) and (3.23);
Z_n, functions of z in equations (3.5) and (3.23).

Greek symbols

α, coefficient of thermal volume expansion;
β, ratio of convective to conductive heat transfer;
δ, boundary layer thickness;
Θ, temperature excess at radius r_{*1} over that at radius er_{*1};
κ, thermal diffusivity of the porous medium;
λ, aspect ratio, b/a; for rectangular and elliptical cavities, ratio of length of vertical axis to that of horizontal axis (note that this usage differs from that in ref. [1]);
ν, kinematic viscosity of the fluid in the porous medium;
Φ_{max}, for rectangular and elliptical cavities, maximum value of dimensionless stream function;

Ψ, Stokes stream function in dimensionless form;
Ψ_{max}, maximum value of Ψ;
Ψ_*, Stokes stream function.

1. INTRODUCTION

A PREVIOUS paper [1] presented exact solutions for small Rayleigh number free convection due to a temperature gradient normal to the gravitational field in 2-dim. porous cavities of various shapes. As well as being relevant to small Rayleigh number flows occurring in practice, these solutions represent natural points of departure for analyses involving regular expansion in the Rayleigh number.

The present paper develops the extension of ref. [1] to the problems of axisymmetric small Rayleigh number free convection in porous cavities. The work is devoted mainly to cylindrical and toroidal cavities, both of arbitrary aspect ratio. As in the previous study, we need only relatively simple mathematics to secure the required exact solutions. Here also we refer specifically to temperature-induced flows, but the modification to solute-induced flows will be evident.

2. FLOW EQUATION FOR AXISYMMETRIC FREE CONVECTION AT SMALL RAYLEIGH NUMBER

The equations governing axisymmetric steady convection within a porous medium induced by a temperature gradient may be written (e.g. [2])

$$r_* \frac{\partial}{\partial r_*}\left(\frac{1}{r_*}\frac{\partial \Psi_*}{\partial r_*}\right) + \frac{\partial^2 \Psi_*}{\partial z_*^2} = \frac{\alpha k g}{\nu} r_* \frac{\partial T_*}{\partial r_*}, \quad (2.1)$$

$$\frac{\partial \Psi_*}{\partial r_*}\frac{\partial T_*}{\partial z_*} - \frac{\partial \Psi_*}{\partial z_*}\frac{\partial T_*}{\partial r_*} = \kappa\left[\frac{\partial}{\partial r_*}\left(r_*\frac{\partial T_*}{\partial r_*}\right) + r_*\frac{\partial^2 T_*}{\partial z_*^2}\right] \quad (2.2)$$

where the Stokes stream function Ψ_* is such that

$$u_* = -\frac{1}{r_*}\frac{\partial \Psi_*}{\partial z_*}, \quad w_* = \frac{1}{r_*}\frac{\partial \Psi_*}{\partial r_*}. \quad (2.3)$$

We introduce the Rayleigh number

$$R = \frac{\alpha k g \Delta T_* L}{\kappa \nu}. \quad (2.4)$$

Then equations (2.1)–(2.3) may be reduced to the dimensionless forms

$$r\frac{\partial}{\partial r}\left(\frac{1}{r}\frac{\partial \Psi}{\partial r}\right) + \frac{\partial^2 \Psi}{\partial z^2} = Rr\frac{\partial T}{\partial r}, \quad (2.5)$$

$$\frac{\partial \Psi}{\partial r}\frac{\partial T}{\partial z} - \frac{\partial \Psi}{\partial z}\frac{\partial T}{\partial r} = \frac{\partial}{\partial r}\left(r\frac{\partial T}{\partial r}\right) + r\frac{\partial^2 T}{\partial z^2}, \quad (2.6)$$

$$u = -\frac{1}{r}\frac{\partial \Psi}{\partial z}, \quad w = \frac{1}{r}\frac{\partial \Psi}{\partial r}. \quad (2.7)$$

Note that

$$\frac{r}{r_*} = \frac{z}{z_*} = \frac{1}{L}; \quad \frac{T}{T_*} = \frac{1}{\Delta T_*}; \quad \frac{\Psi}{\Psi_*} = \frac{1}{L\kappa}; \quad \frac{u}{u_*} = \frac{w}{w_*} = \frac{L}{\kappa}. \quad (2.8)$$

When R is so small that heat transfer by conduction dominates that due to convection, the RHS of equation (2.6) may be set equal to zero. If then the steady radial heat flux per unit axial length is constant and equal to Q, we have

$$Q = -2\pi c \kappa r_* \frac{\partial T_*}{\partial r_*} \quad (2.9)$$

where c is the volumetric heat capacity. It then follows that

$$r_*\frac{\partial T_*}{\partial r_*} = \frac{\partial T_*}{\partial \ln r_*} = \text{constant} = -\frac{Q}{2\pi c\kappa} = -\Theta \quad (2.10)$$

where Θ is the temperature excess at radius $r_* = r_{*1}$ over that at radius $r_* = e r_{*1}$. Θ is thus a characteristic macroscopic radial temperature difference and may be identified with ΔT_*. Note that we limit ourselves here to the simplest axisymmetric thermal field. The field (2.10) would be disturbed, for example, if there were large differences between the thermal diffusivity of the porous medium and that of the surrounding material.

In the previous study [1], we identified the characteristic length L with the square root of the cavity cross-sectional area. Analogously, we here identify L with $A^{1/2}$, where A is the area of the radial cross-section of the cavity. Accordingly, with equation (2.4) restated in the form

$$R = \frac{\alpha k g \Theta A^{1/2}}{\kappa \nu}, \quad (2.11)$$

we may finally express equation (2.5) as

$$r\frac{\partial}{\partial r}\left(\frac{1}{r}\frac{\partial \Psi}{\partial r}\right) + \frac{\partial^2 \Psi}{\partial z^2} + R = 0. \quad (2.12)$$

3. SOLUTION FOR CYLINDRICAL CAVITIES

We consider the cavity bounded by the cylindrical surface $r_* = a$ and the planes $z_* = \pm \frac{1}{2}b$. We note that $L = A^{1/2} = (ab)^{1/2}$. Then equation (2.12) is subject to the conditions

$$\Psi = 0, \quad r \leqslant \lambda^{-1/2}, \quad z = \pm \tfrac{1}{2}\lambda^{1/2}; \qquad \Psi = 0, \quad r = 0 \text{ and } \lambda^{-1/2}, \quad |z| < \lambda^{1/2}. \quad (3.1)$$

Here $\lambda = b/a$ is the aspect ratio.

3.1. *Exact solution*

We now write

$$\Psi(r, z) = \tfrac{1}{2}R[\tfrac{1}{4}\lambda - z^2 + f(r, z)] \quad (3.2)$$

so that

$$r\frac{\partial}{\partial r}\left(\frac{1}{r}\frac{\partial f}{\partial r}\right) + \frac{\partial^2 f}{\partial z^2} = 0, \quad (3.3)$$

subject to the conditions

$$f = 0, \quad r \leqslant \lambda^{-1/2}, \quad z = \pm \tfrac{1}{2}\lambda^{1/2},$$
$$f = z^2 - \tfrac{1}{4}\lambda, \quad r = 0 \quad \text{and} \quad \lambda^{-1/2}, \quad |z| < \tfrac{1}{2}\lambda^{1/2}. \tag{3.4}$$

We use separation of variables to solve equation (3.3) subject to conditions (3.4) in the form

$$\sum_{n=0}^{\infty} Y_n(r) \cdot Z_n(z).$$

We require that each Y_n and Z_n satisfy

$$\frac{r}{Y_n}\frac{\mathrm{d}}{\mathrm{d}r}\left(\frac{1}{r}\frac{\mathrm{d}Y_n}{\mathrm{d}r}\right) = -\frac{1}{Z_n}\frac{\mathrm{d}^2 Z_n}{\mathrm{d}Z^2} = c_n^2, \tag{3.5}$$

with c_n a constant. We note that for

$$c_n = (2n+1)\pi\lambda^{-1/2}, \tag{3.6}$$

with n a non-negative integer, the function

$$Z_n(z) = \cos(c_n z) \tag{3.7}$$

satisfies equation (3.5) and vanishes on $z = \pm \frac{1}{2}\lambda$, as required by the first of the conditions (3.4). It then follows from conditions (3.4) and equation (3.5) that

$$Y_n(r) = r[A_n I_1(c_n r) + B_n K_1(c_n r)]. \tag{3.8}$$

We thus arrive at the solution

$$f(r, z) = r \sum_{n=0}^{\infty} \cos(c_n z)[A_n I_1(c_n r) + B_n K_1(c_n r)]. \tag{3.9}$$

The second of conditions (3.4) requires that

$$z^2 - \tfrac{1}{4}\lambda = \lim_{r \to 0}\left\{ r \sum_{n=0}^{\infty} \cos(c_n z) \times [A_n I_1(c_n r) + B_n K_1(c_n r)]\right\} \tag{3.10}$$

and

$$z^2 - \tfrac{1}{4}\lambda = \lambda^{-1/2} \sum_{n=0}^{\infty} \cos(c_n z)[A_n I_1(c_n \lambda^{-1/2}) + B_n K_1(c_n \lambda^{-1/2})]. \tag{3.11}$$

We find from Fourier analysis also that, in $|z| \leqslant \frac{1}{2}\lambda$,

$$z^2 - \tfrac{1}{4}\lambda = \sum_{n=0}^{\infty}{}' C_n \cos(c_n z) \tag{3.12}$$

with

$$C_n = (-1)^{n+1}\frac{8\lambda}{\pi^3(2n+1)^3}. \tag{3.13}$$

The coefficient of $\cos(c_n z)$ in all three of the expansions (3.10)–(3.12) must be equal; and it follows that

$$B_n = c_n C_n,$$

$$A_n = \frac{C_n}{I_1(c_n\lambda^{-1/2})}[\lambda^{1/2} - c_n K_1(c_n\lambda^{-1/2})]. \tag{3.14}$$

The solution is therefore

$$f(r, z) = r \sum_{n=0}^{\infty}{}' C_n \cos(c_n z) \times \left[\frac{\lambda^{1/2} - c_n K_1(c_n\lambda^{-1/2})}{I_1(c_n\lambda^{-1/2})} I_1(c_n r) + c_n K_1(c_n r)\right] \tag{3.15}$$

Combining equations (3.2), (3.6), (3.13) and (3.15), we obtain the solution for Ψ

$$\Psi(r, z) = \frac{R\lambda}{8}\left\{1 - \frac{4z^2}{\pi} - \frac{32r}{\pi^2\lambda^{1/2}} \times \sum_{n=0}^{\infty}{}' (-1)^n \frac{\cos[(2n+1)\pi\lambda^{-1/2}z]}{(2n+1)^2} \times \left[\left\{\frac{\lambda}{(2n+1)\pi} - K_1[(2n+1)\pi\lambda^{-1}]\right\} \times \frac{I_1[(2n+1)\pi\lambda^{-1/2}r]}{I_1[(2n+1)\pi\lambda^{-1}]} + K_1[(2n+1)\pi\lambda^{-1/2}r]\right]\right\}. \tag{3.16}$$

The solution on the midplane is

$$\Psi(r, 0) = \frac{R}{8}\left\{1 - \frac{32r}{\pi^2\lambda^{1/2}} \sum_{n=0}^{\infty}{}' \frac{(-1)^n}{(2n+1)^2} \times \left[\left\{\frac{\lambda}{(2n+1)\pi} - K_1[(2n+1)\pi\lambda^{-1}]\right\} \times \frac{I_1[(2n+1)\pi\lambda^{-1/2}r]}{I_1[(2n+1)\pi\lambda^{-1}]} + K_1[(2n+1)\pi\lambda^{-1/2}r]\right]\right\}. \tag{3.17}$$

The series in equation (3.16) is rapidly convergent for λ small; and, in fact, it converges conveniently even for λ as large as 4 (Fig. 3).

3.2. *Core flow and boundary layers for small* λ

It is of some interest to examine equation (3.16) in the limit as $\lambda \to 0$. For small enough λ the leading term of the summation dominates and we have

$$\Psi(r, z) \approx \frac{R\lambda}{8}\left\{1 - \frac{4z^2}{\lambda} - \frac{32r\cos[\pi\lambda^{-1/2}z]}{\pi^2\lambda^{1/2}} \times \left[\left\{\frac{\lambda}{\pi} - K_1\left(\frac{\pi}{\lambda}\right)\right\}\frac{I_1[\pi\lambda^{-1/2}r]}{I_1[\pi/\lambda]} + K_1[\pi\lambda^{-1/2}r]\right]\right\}. \tag{3.18}$$

We see that, for small λ, the whole cavity is occupied by the core flow

$$\Psi \approx \frac{R\lambda}{8}\left[1 - \frac{4z^2}{\lambda}\right],$$

except for two boundary layer regions, one about the axis $r = 0$, and one on the external cylindrical boundary $r = \lambda^{-1/2}$. The axial boundary layer is dominated by the term in $K_1[\pi\lambda^{-1/2}r]$, and its radius is accordingly $O(\lambda^{1/2})$; and the outer boundary layer is dominated by the term in $I_1[\pi\lambda^{-1/2}r]$ so that its thickness is also $O(\lambda^{1/2})$ (Fig. 1). We note also that in this limit of λ small

$$\Psi_{\max} \approx R\lambda/8. \tag{3.19}$$

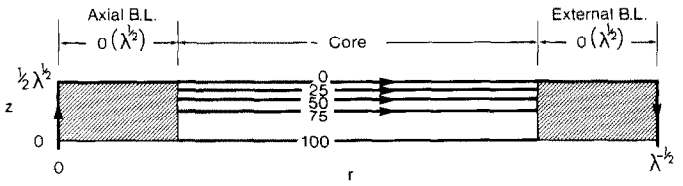

FIG. 1. Free convection at small Rayleigh number in cylindrical cavities. Structure of core flow and boundary layers for aspect ratio λ small. Numerals on Stokes streamlines in core are values of $800\,\Psi(R\lambda)$.

3.3. *Second form of exact solution efficient for large* λ

Alternatively, we may write

$$\Psi(r, z) = \tfrac{1}{2}R[h(r, z) - r^2 \ln(\lambda^{1/2} r)] \quad (3.20)$$

so that equations (2.12) and (3.1) reduce to

$$r\frac{\partial}{\partial r}\left(\frac{1}{r}\frac{\partial h}{\partial r}\right) + \frac{\partial^2 h}{\partial z^2} = 0, \quad (3.21)$$

subject to the conditions

$$h = r^2 \ln(\lambda^{1/2} r), \quad 0 \leqslant r \leqslant \lambda^{-1/2}, \quad z = \pm \tfrac{1}{2}\lambda^{1/2};$$
$$h = 0, \quad r = 0 \quad \text{and} \quad \lambda^{-1/2}, \quad |z| < \tfrac{1}{2}\lambda^{1/2}. \quad (3.22)$$

Separation of variables yields the solution of equations (3.21) and (3.22) in the form

$$\sum_{n=1}^{\infty} Y_n(r) \cdot Z_n(z).$$

We require that each Y_n and Z_n satisfy

$$\frac{r}{Y_n}\frac{\mathrm{d}}{\mathrm{d}r}\left(\frac{1}{r}\frac{\mathrm{d}Y_n}{\mathrm{d}r}\right) = -\frac{1}{Z_n}\frac{\mathrm{d}^2 Z_n}{\mathrm{d}z^2} = -c_n^2. \quad (3.23)$$

We note that for

$$c_n = \lambda^{1/2} j_n, \quad (3.24)$$

where j_n is the nth positive zero of J_1,

$$Y_n(r) = rJ_1(c_n r) \quad (3.25)$$

satisfies equation (3.23) and vanishes on $r = 0$ and $\lambda^{-1/2}$, as required by the second condition of equations (3.22). It then follows from equations (3.22) and (3.23) that

$$Z_n(z) = A_n \cosh(c_n z), \quad (3.26)$$

since Ψ (and hence Z_n) is necessarily an even function of z. We thus obtain the solution

$$h(r, z) = r\sum_{n=1}^{\infty} A_n \cosh(c_n z) J_1(c_n r). \quad (3.27)$$

The first of conditions (3.22) requires that

$$r \ln(\lambda^{1/2} r) = \sum_{n=1}^{\infty} A_n \cosh(\tfrac{1}{2}c_n \lambda^{1/2}) J_1(c_n r); \quad (3.28)$$

and we find from the Fourier–Bessel expansion (e.g. [3]) that

$$r \ln(\lambda^{1/2} r) = \sum_{n=1}^{\infty} C_n J_1(c_n r) \quad (3.29)$$

with

$$C_n = \frac{2\lambda^{1/2}\mathscr{I}_n}{J_2^2(j_n)}. \quad (3.30)$$

Here

$$\mathscr{I}_n = \int_0^1 v^2 \ln v\, J_1(j_n v)\mathrm{d}v. \quad (3.31)$$

Equating coefficients in equations (3.28) and (3.29), we find

$$A_n = \frac{2\lambda^{1/2}\mathscr{I}_n}{J_2^2(j_n)\cosh(\frac{1}{2}\lambda j_n)}. \quad (3.32)$$

The solution for Ψ is thus

$$\Psi(r, z) = \frac{Rr}{2}\left[-r \ln(\lambda^{1/2} r) + \sum_{n=1}^{\infty} A_n \cosh(c_n z) J_1(c_n r)\right], \quad (3.33)$$

with A_n and c_n given by equations (3.32) and (3.24). The series in equation (3.33) converges rapidly for λ large, thus providing an efficient means of evaluating Ψ in that case.

3.4. *Core flow and boundary layers for large* λ

When λ is large enough, the leading term of the series dominates and

$$\Psi(r, z) \approx \frac{Rr}{2}\left[-r \ln(\lambda^{1/2} r) + \frac{2\lambda^{1/2}\cosh(\lambda^{1/2} j_1 z) J_1(\lambda^{1/2} j_1 r)}{J_2^2(j_1)\cosh(\frac{1}{2}\lambda j_1)}\right]. \quad (3.34)$$

For large λ the whole cavity is occupied by the core flow $\Psi \approx -\frac{1}{2}Rr^2 \ln(\lambda^{1/2} r)$, except for the boundary layers on the top and bottom bounding planes $z = \pm \frac{1}{2}\lambda^{1/2}$. Only within these boundary layers is the second term in the square bracket of equation (3.34) significant. This requires that the factor $\cosh(\lambda^{1/2} j_1 z)/\cosh(\frac{1}{2}\lambda j_1)$ be not negligibly small with respect to unity. Accordingly, $\lambda^{1/2} j_1 \delta = O(1)$, where δ is the boundary layer thickness. Since $j_1 \approx 3.83$, this implies that $\delta = O(\lambda^{-1/2})$ (Fig. 2).

It is readily shown by differentiating equation (3.34) with respect to r that, in the limit of large λ, the maximum value of Ψ is

$$\Psi_{\max} \approx R/(4\mathrm{e}\lambda), \quad (3.35)$$

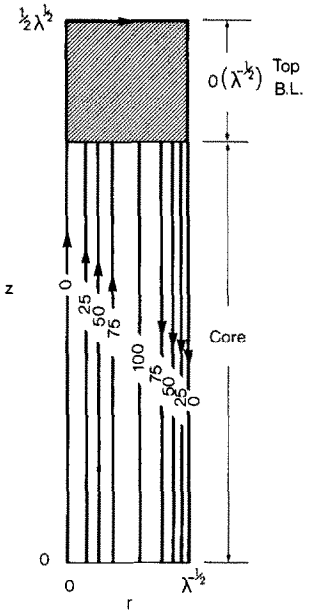

FIG. 2. Free convection at small Rayleigh number in cylindrical cavities. Structure of core flow and boundary layers for aspect ratio λ large. Numerals on Stokes streamlines in core are values of $400\,e\lambda\Psi/R$.

and that this occurs at

$$r = 0, \quad z \approx (e\lambda)^{-1/2}. \tag{3.36}$$

3.5. *Illustrative results*

Figure 3 depicts the Stokes stream function for cylindrical cavities in the dimensionless form $R^{-1}\Psi(r, z)$ for $\lambda = 0.25, 0.5, 1, 2$, and 4. The plots are based on calculations using the first few terms of equation (3.16): even for $\lambda = 4$ truncating the series at $n = 3$ gave adequate accuracy.

It will be seen that, for λ as large as 0.25, there is already some suggestion of the core flow and boundary layers for small λ depicted in Fig. 1; and similarly the plot for λ as small as 4 already approaches the core flow and boundary layer pattern for large λ shown in Fig. 2.

4. SOLUTION FOR TOROIDAL CAVITIES

The previous study of 2-dim. free convection at small Rayleigh number [1] revealed that the exact solution for elliptical cavities was mathematically elementary and, in particular, much simpler than that for rectangular cavities. Similarly, we find here that the solution for toroidal cavities is elementary and simpler than that for cylindrical cavities.

We consider the toroidal cavity with radial cross-section consisting of the primary logarithmic oval with horizontal and vertical axes of length a and b, respectively. We refer to a toroid with this cross-section as a *primary logarithmic toroid.* Various relevant properties of primary and secondary logarithmic ovals are set out in the Appendix.

We then have equation (2.12) subject to the condition that $\Psi = 0$ on the toroid

$$-e\lambda^2 r^2 \ln\frac{(\pi e)^{1/4}\lambda^{1/2} r}{2} - 2z^2 = 0. \tag{4.1}$$

We have, as before, that the aspect ratio $\lambda = b/a$. The solution of equation (2.12) satisfying condition (4.1) is

$$\Psi = \frac{-R}{2(e\lambda^2 + 2)}\left(e\lambda^2 r^2 \ln\frac{(\pi e)^{1/4}\lambda^{1/2} r}{2} + 2z^2\right). \tag{4.2}$$

Figure 4 is a dimensionless plot of the Stokes stream function in the form $10(\pi e)^{1/2}(e\lambda^2 + 2)\Psi/R$ as a function of the coordinates $(\lambda^{1/2}r, \lambda^{-1/2}z)$. Equation (4.2) implies that the maximum value of Ψ, Ψ_{max}, occurs at $(r, z) = (2\pi^{-1/2} e^{-3/4} \lambda^{-1/2}, 0)$, and that

$$\Psi_{max} = \frac{R\lambda}{(\pi e)^{1/2}(e\lambda^2 + 2)}. \tag{4.3}$$

It follows from the properties of logarithmic ovals established in the Appendix that as Ψ increases from 0 to Ψ_{max}, the aspect ratio of the streamlines increases from λ to $\lambda(e/2)^{1/2}$; and that their shape changes systematically from that of a primary logarithmic oval to that of an ellipse.

5. SIMPLE EXACT SOLUTIONS FOR OTHER CONFIGURATIONS

Various other simple exact solutions exist for axisymmetric free convection at small Rayleigh number. These are for configurations of the porous solid in which the radial cross-section is bounded by a logarithmic variant of a conic section, with r_*^2 in the equation of the conic section replaced by $r_*^2 \ln(r_*/a)$ and adjustments of sign where required. In this way one may, for example, secure solutions in which the bounding surfaces and stream surfaces are 'logarithmic' paraboloids and hyperboloids of revolution. In general these are of limited physical interest. They involve infinite flow regions, and the large Reynolds numbers in the far flow field prejudice the applicability of the present small Rayleigh number analysis.

These objections do not hold, however, for toroidal cavities. The primary logarithmic toroid considered in Section 4 had internal radius $r_{*0} = 0$. Solutions are available also for cases where $r_{*0} \neq 0$ and the cross-section is a *secondary* logarithmic oval (see Appendix). In view of result (A10), the solution approaches that for the 2-dim. elliptical cavity (Section 4 of ref. [1]) in the limit of large r_{*0}/a. This is physically obvious, since as $r_{*0}/a \to \infty$ any finite sector of the toroid becomes indistinguishable from a long cylinder of elliptical cross-section with a linear temperature gradient across it.

6. VARIATION OF $R^{-1}\Psi_{max}$ WITH CAVITY SHAPE

The quantity $R^{-1}\Psi_{max}$ is a measure of the relative strength of free convection at small R in a particular axisymmetric porous cavity. It is of interest to examine the dependence of $R^{-1}\Psi_{max}$ on cavity shape and on the aspect ratio λ. In Fig. 5 we compare the variation of $R^{-1}\Psi_{max}$ with λ for cylindrical and toroidal cavities.

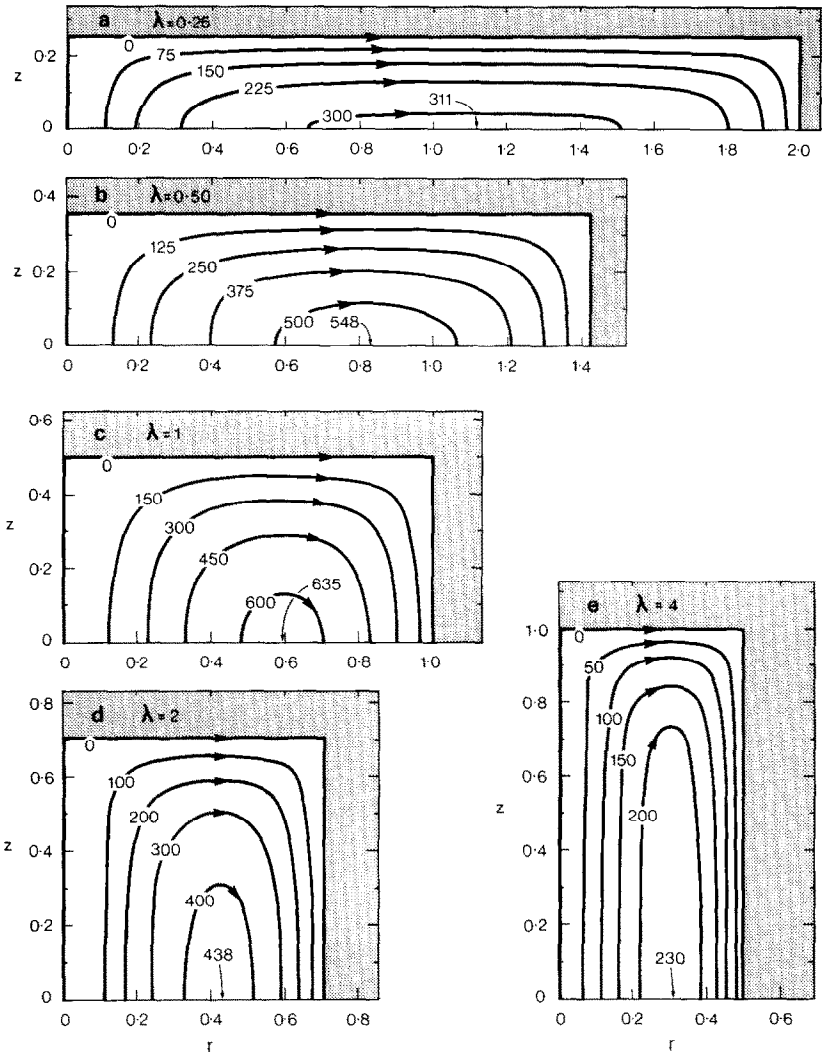

FIG. 3. Free convection at small Rayleigh number in cylindrical cavities. Dimensionless plot of the Stokes stream function for aspect ratio λ = (a) 0.25, (b) 0.5, (c) 1, (d) 2, and (e) 4. Numerals on the curves are values of $10^4\,\Psi/R$.

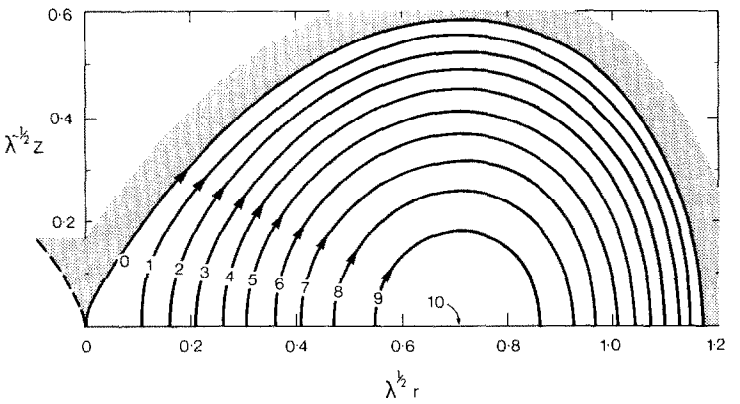

FIG. 4. Free convection at small Rayleigh number in toroidal cavities. Plot of the Stokes stream function in the dimensionless form $10(\pi e)^{1/2}\,(e\lambda^2 + 2)\,\Psi/R$. The coordinates are $\lambda^{1/2}r$, $\lambda^{-1/2}z$. Note that the plot is invariant with respect to the aspect ratio λ.

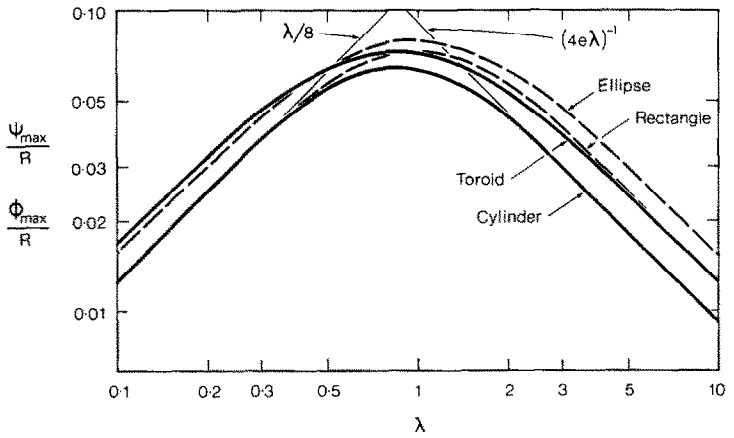

FIG. 5. Free convection at small Rayleigh number in axisymmetric and 2-dim. cavities of various shapes. Dependence of the strength of convection on the aspect ratio λ. The variation of Ψ_{max}/R for cylindrical and toroidal cavities shown as full curves. Asymptotic behaviour for cylindrical cavities is also shown. The variation of Φ_{max}/R for rectangular and elliptical cavities shown as broken curves.

We show on this figure also the variation of $R^{-1}\Phi_{max}$ with λ for 2-dim. free convection in rectangular and elliptical porous cavities [1]. Φ_{max} is the maximum value of the dimensionless stream function. Note that in view of the orientation-invariance theorem for 2-dim. convection [1], $\Phi_{max}(\lambda^{-1}) = \Phi_{max}(\lambda)$. In cylindrical cavities variation with λ of the position of Ψ_{max}, i.e. of the centre of the toroidal convective roll, is also of interest (Fig. 6).

6.1. *Cylindrical cavities: dependence of* $R^{-1}\Psi_{max}$ *on* λ

Note the asymptotes $R^{-1}\Psi_{max} = \lambda/8$ as $\lambda \to 0$, and $R^{-1}\Psi_{max} = (4e\lambda)^{-1}$ as $\lambda \to \infty$ (Fig. 5).

6.2. *Cylindrical cavities: position of* Ψ_{max}

We denote by $(r, z) = (r_1, 0)$ the position of Ψ_{max} (Fig. 6). The quantity $\lambda^{1/2}r_1$ expresses the position as a fraction of cavity radius. Although our calculations give only approximate values of $\lambda^{1/2}r_1$, they indicate that this quantity remains close to its value as $\lambda \to \infty$, 0.6065, for λ as small as 1. It decreases to about 0.56 as λ decreases to 0.25.

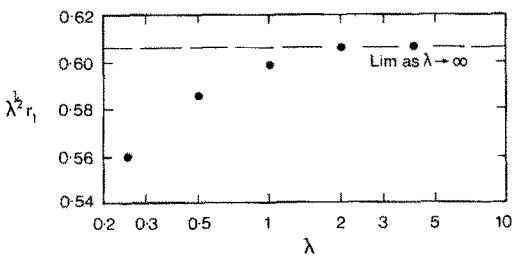

FIG. 6. Free convection at small Rayleigh number in cylindrical cavities. Dependence on aspect ratio λ of the position of the centre of the convective roll. This is at $(r, z) = (r_1, 0)$, where $\Psi = \Psi_{max}$. Note that $\lambda^{1/2}r_1$ expresses the position as a fraction of cavity radius.

6.3. *Toroidal cavities: dependence of* $R^{-1}\Psi_{max}$ *on* λ

It follows from equation (4.2) that Ψ_{max} occurs at $(r, z) = (2\pi^{-1/2}e^{-3/4}\lambda^{-1/2}, 0)$, and that

$$\Psi_{max} = \frac{R\lambda}{(\pi e)^{1/2}(e\lambda^2 + 2)}. \tag{6.1}$$

It is simply shown that Ψ_{max} for toroidal cavities has its maximum value $(8\pi e^2)^{-1/2} \approx 0.07338$ when $\lambda = (2/e)^{1/2} \approx 0.8578$ (Fig. 5).

6.4. *Discussion*

It is of interest to compare the results brought together in Fig. 5. All four curves are essentially similar. The curve for toroidal cavities has its maximum at, and is symmetrical about, $\lambda = (2/e)^{1/2}$. The curve for cylindrical cavities appears also to have its maximum at, and to exhibit symmetry about, $\lambda = (2/e)^{1/2}$. The maximum value for cylinders is about 0.065, rather less than for toroids. Analogous relationships hold for 2-dim. cavities: for both elliptical and rectangular cavities $R^{-1}\Phi_{max}$ is symmetrical about $\lambda = 1$ and has its maximum there. The maximum for rectangles, 0.0737, is somewhat less than that for ellipses, 0.0796.

7. RELATIVE MAGNITUDE OF CONVECTION AND CONDUCTION. CRITICAL R

We now examine the relative magnitude of convective and conductive heat transport in axisymmetric systems. This provides estimates of the critical Rayleigh number for applicability of the present analysis (cf. [1]). We take as the measure of convective transport the quantity H, the total convection of heat within the cavity across its mid-plane $r_* \leqslant a, z_* = 0$. Then, for both toroidal and cylindrical cavities, we have

$$H = 2\pi c \int_0^a \frac{\partial \Psi_*}{\partial r_*}(r_*, 0)\, T_*(r_*)\, dr_*. \tag{7.1}$$

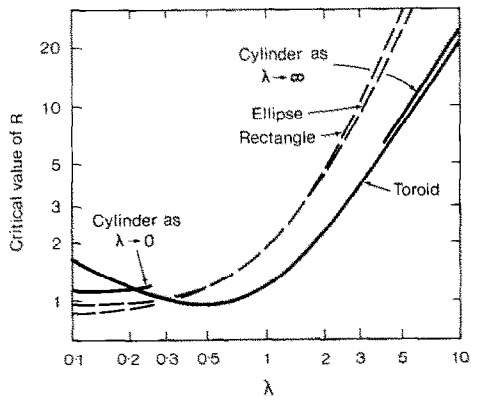

FIG. 7. Free convection at small Rayleigh number in axisymmetric and 2-dim. cavities of various shapes. Dependence on the aspect ratio λ of the critical value of R for applicability of the small Rayleigh number analysis. Relation for toroidal cavities and asymptotic behaviour for cylindrical cavities shown as full curves. Relations for rectangular and elliptical cavities shown as broken curves.

Integration of equation (2.10) yields

$$T_*(r_*) = -\frac{Q}{2\pi c\kappa}\ln\frac{r_*}{a}, \tag{7.2}$$

with a convenient value taken for the arbitrary integration constant. Putting equation (7.2) into equation (7.1) and using the third of equations (2.8), we find that

$$H = -QA^{1/2}\int_0^{A^{-1/2}a}\frac{\partial\Psi}{\partial r}(r, 0)\,\ln[r/A^{-1/2}a)]\,\mathrm{d}r. \tag{7.3}$$

7.2. *Toroidal cavities: critical* R

Using equation (4.2) in equation (7.3) and performing the integration, we find that

$$H = QA^{1/2}\frac{Re\lambda}{2(\pi e)^{1/2}(e\lambda^2+2)}. \tag{7.4}$$

For toroidal cavities we take as the measure of conductive transport the quantity K, the total radial heat conduction within the cavity across the cylinder $r_* = e^{-1/2}a$. Evidently

$$K = Qb = 2(\pi e)^{-1/4}\lambda^{1/2}QA^{1/2}. \tag{7.5}$$

We introduce the ratio $\beta = H/K$ as the measure of the relative importance of convective and conductive heat transport in the system. It then follows from equations (7.4) and (7.5) that

$$\beta = \frac{Re^{3/4}\lambda^{1/2}}{4\pi^{1/4}(e\lambda^2+2)}. \tag{7.6}$$

Applicability of the present analysis requires that convective heat transfer be small compared with conductive heat transfer, i.e., say, that $\beta < 0.1$. We thus obtain the criterion

$$R < R_1 = \frac{2\pi^{1/4}(e\lambda^2+2)}{5e^{3/4}\lambda^{1/2}}. \tag{7.7}$$

The critical value of R, R_1, has its minimum value

$$\frac{16}{15}\left(\frac{3\pi}{2e^2}\right)^{1/4} \approx 0.9532$$

when $\lambda = (2/3e)^{1/2} \approx 0.4952$. As $\lambda \to \infty$, R_1 behaves like $\frac{2}{5}(\pi e)^{1/4}\lambda^{3/2} \approx 0.6838\lambda^{3/2}$; and as $\lambda \to 0$, R_1 behaves like

$$\frac{4\pi^{1/4}}{5e^{3/4}}\lambda^{-1/2} \approx 0.5031\lambda^{-1/2} \text{ (Fig. 7).}$$

7.3. *Cylindrical cavities: critical* R

For cylindrical cavities equation (7.3) reduces to

$$H = -QA^{1/2}\int_0^{\lambda^{1/2}}\frac{\partial\Psi}{\partial r}(r, 0)\ln(\lambda^{1/2}r)\,\mathrm{d}r. \tag{7.8}$$

General expressions for H may be found by using equations (3.18) or (3.33) in equation (7.8) and performing the integration. The results are complicated and we limit ourselves here to examining H in the limits of small and large λ.

When λ is small, convective heat transport is concentrated in the axial boundary layer (Section 3.2). Within this boundary layer

$$\Psi(r, 0) \approx \frac{R\lambda}{8}\left[1 - \frac{\pi r}{\lambda^{1/2}}K_1\left(\frac{\pi r}{\lambda^{1/2}}\right)\right] \approx -\frac{\pi^2 R}{16}r^2\ln\frac{\pi r}{2\lambda^{1/2}}. \tag{7.9}$$

Accordingly, limiting the integration to the axial boundary layer, we find

$$H \approx QA^{1/2}\frac{\pi^2 R}{16}\int_0^{(2\lambda^{1/2})/(\pi e^{1/2})}\frac{\mathrm{d}}{\mathrm{d}r}\left(r^2\ln\frac{\pi r}{2\lambda^{1/2}}\right)\ln(\lambda^{1/2}r)\,\mathrm{d}r = -QA^{1/2}\frac{R\lambda}{8}\ln[(2\lambda e^{1/2})/\pi]. \tag{7.10}$$

For cylindrical cavities we define K as the total radial heat conduction in the cavity, so that

$$K = Qb = \lambda^{1/2}QA^{1/2}. \tag{7.11}$$

It follows from equations (7.10) and (7.11) that, for λ small,

$$\beta \approx -\frac{R\lambda^{1/2}}{8}\ln\frac{2\lambda e^{1/2}}{\pi}. \tag{7.12}$$

This yields the following criterion on R for cylindrical cavities

$$\lambda \text{ small}, R < R_1 \approx -\frac{4\lambda^{-1/2}}{5\ln[(2\lambda e^{1/2})/\pi]}. \tag{7.13}$$

On the other hand, when λ is large (Section 3.4),

$$\Psi(r, 0) \approx -\tfrac{1}{2}Rr^2\ln(\lambda^{1/2}r). \tag{7.14}$$

Putting equation (7.14) in equation (7.8) and integrating, we find

$$H \approx QA^{1/2}\frac{R}{8\lambda}. \tag{7.15}$$

Combining this with equation (7.11) gives

$$\beta \approx \frac{R}{8}\lambda^{-3/2}. \tag{7.16}$$

We thus obtain the criterion on R for cylindrical cavities:

$$\lambda \text{ large}, \quad R < R_1 \approx \frac{4}{5}\lambda^{3/2}. \tag{7.17}$$

The behaviour of R_1 in the limits of small λ, equation (7.13), and large λ, equation (7.17), is shown in Fig. 7.

7.4. *Discussion*

In Fig. 7 we bring together results for cavities of various shapes on the variation with λ of the critical value of R below which the small Rayleigh number analysis is applicable. As well as the present results for toroidal and cylindrical cavities, we show also those found [1] for elliptical and rectangular cavities.

The behaviour for toroids and cylinders is generally similar. For both cavity shapes $R_1 \propto \lambda^{3/2}$ as $\lambda \to \infty$; in each case R_1 passes through a minimum value of about 1 (at $\lambda \approx 0.5$ for toroids and at $\lambda \approx 0.12$ for cylinders); and it then increases comparatively slowly as λ decreases to 0: as $\lambda^{-1/2}$ for toroids and as $\lambda^{-1/2}(-\ln\lambda)^{-1}$ for cylinders. In both cases $R_1 = O(1)$ in $0.1 \leqslant \lambda \leqslant 1$.

These results are broadly similar to, and consistent with, those for 2-dim. cavities [1]. For both elliptical and rectangular cavities, however, the increase as $\lambda \to \infty$ is as λ^2, and there is a slow decrease to a constant asymptotic value as $\lambda \to 0$.

8. CORE FLOWS AND BOUNDARY LAYERS IN AXISYMMETRIC AND TWO-DIMENSIONAL CAVITIES

8.1. *Cylindrical cavities*

We have seen in Section 3 that in the limit both as $\lambda \to 0$ and as $\lambda \to \infty$ the small R convective flow pattern in cylindrical cavities tends towards a core flow with two boundary layers. For $\lambda \to 0$, the core flow is a horizontal parallel flow, with one boundary layer on the axis and a second on the external cylindrical boundary (Fig. 1). For both boundary layers $\delta = O(\lambda^{1/2})$. (The analysis leading to equation (7.9) gives $\delta \approx (2/\pi)\lambda^{1/2}$ for the axial layer.) For $\lambda \to \infty$, the core flow is a vertical parallel flow, with boundary layers of thickness $O(\lambda^{-1/2})$ on the top and bottom bounding planes (Fig. 2).

8.2. *Rectangular cavities*

The solution for small R convection in rectangular cavities [1] leads similarly to a core flow with two boundary layers in the limits both as $\lambda \to 0$ and as $\lambda \to \infty$. An analysis similar to that of Sections 3.2 and 3.4 shows that as $\lambda \to 0$ the solution tends towards a horizontal parallel core flow with boundary layers of thickness $O(\lambda^{1/2})$ on the two vertical bounding walls; and that as $\lambda \to \infty$ the solution tends towards a vertical parallel core flow with boundary layers of thickness $O(\lambda^{-1/2})$ on the two horizontal bounding walls.

8.3. *Toroidal and elliptical cavities: flow patterns invariant with* λ

The solutions for toroidal (Section 4) and elliptical [1] cavities are in marked contrast to the foregoing. The toroidal solution, equation (4.2), may readily be rewritten as

$$\frac{\Psi}{\Psi_{\max}} = -\frac{(\pi e)^{1/2}}{2}\left[e\,(\lambda^{1/2}r)^2 \ln\frac{(\pi e)^{1/2}(\lambda^{1/2}r)}{2} + 2(\lambda^{-1/2}z)^2\right]. \tag{8.1}$$

Plotted against the coordinates $(\lambda^{1/2}r, \lambda^{-1/2}z)$, the flow pattern is invariant with respect to variation of λ (Fig. 4). Evidently no pattern of core flow and boundary layers can emerge here in the limits $\lambda \to 0$ or ∞.

Similarly the elliptical solution (equation (4.2) of ref. [1]) yields a plot of the flow pattern which is invariant with respect to variation of λ. In that case also no pattern of core flow and boundary layers can emerge.

8.4. *The geometrical origin of cores and boundary layers at small* R

The existence of cores and boundary layers in the cases treated in Sections 8.1 and 8.2, and their absence from those of Section 8.3, indicates their geometrical origin. Cores and boundary layers emerging in axisymmetric and 2-dim. free convection at small Rayleigh number are essentially artifacts of cavity geometry: they are not inherent in the physics.

The various solutions developed here and in ref. [1] are consistent with the following interpretation for cavities of shapes other than toroidal or elliptical. Consider a sequence of cavities, all of the same basic shape, but with the aspect ratio λ free to vary. Then, for axisymmetric systems with λ about unity, the flow field is essentially that for the toroidal cavity, equation (4.2), the effect of the particular cavity geometry being limited to adjustments near the boundaries. On the other hand, the influence of the boundary geometry becomes dominant both as $\lambda \to 0$ and as $\lambda \to \infty$, and a core/boundary layer flow emerges. For 2-dim. cavities the interpretation is similar, except that in this case the flow with λ about unity is basically that for the elliptical cavity (equation (4.2) of ref. [1]).

8.5. *The special character of toroidal and elliptical cavities*

The foregoing considerations indicate the special character of the toroidal and elliptical solutions. They represent, respectively, fundamental axisymmetric and 2-dim. flow patterns for convection at small R. They describe the basic axisymmetric toroidal convective roll, and the basic 2-dim. elliptic convective roll; and they lead naturally to regular expansions in R, a matter to be pursued in a later paper.

REFERENCES

1. J. R. Philip, Free convection at small Rayleigh number in porous cavities of rectangular, elliptical, triangular and other cross-sections, *Int. J. Heat Mass Transfer* **25**, 1503–1509 (1982).
2. C.-S. Yih, *Dynamics of Nonhomogeneous Fluids*, p. 238. Macmillan, New York (1965).
3. G. N. Watson, *A Treatise on the Theory of Bessel Functions*, (2nd edn) p. 576. Cambridge University Press (1958).

APPENDIX
THE LOGARITHMIC OVAL

The curve

$$-\mathrm{e}\,r_*^2 \ln r_* - 2z_*^2 = 0 \tag{A1}$$

is a *logarithmic oval* with horizontal axis of unit length running from $(r_*, z_*) = (0, 0)$ to $(1, 0)$, and with vertical axis of unit length running from $(\mathrm{e}^{-1/2}, -\frac{1}{2})$ to $(\mathrm{e}^{-1/2}, \frac{1}{2})$. The aspect ratio, λ, is equal to 1. It is readily shown by integration that the area of the oval, equation (A1),

$$A = \tfrac{1}{4}(\pi\mathrm{e})^{1/2} \tag{A2}$$

More generally, the curve

$$-\mathrm{e}\frac{r_*^2}{a^2} \ln \frac{r_*}{a} - 2\frac{z_*^2}{b^2} = 0 \tag{A3}$$

is a logarithmic oval with horizontal axis of length a and with vertical axis of length b. The aspect ratio, λ, is equal to b/a. The area of the oval is then

$$A = \frac{(\pi\mathrm{e})^{1/2}}{4} ab. \tag{A4}$$

We refer to all ovals describable by an equation of the form (A3) as *primary logarithmic ovals*. On the other hand, the set of curves parametrized by E^2

$$-\mathrm{e}\frac{r_*^2}{a} \ln \frac{r_*}{a} - 2\frac{z_*^2}{b^2} = E^2, \quad 0 \leqslant E^2 \leqslant \tfrac{1}{2} \tag{A5}$$

represents a nested set of ovals. We refer to all ovals satisfying (A5) for $E^2 > 0$ as *secondary logarithmic ovals*.

Taking $L = A^{1/2}$ here, as before, we use the first of equations (2.8) to rewrite (A3) and (A5) in the dimensionless forms

$$-\mathrm{e}\lambda^2 r^2 \ln \frac{(\pi\mathrm{e})^{1/4}\lambda^{1/2} r}{2} - 2z^2 = 0, \tag{A6}$$

$$-\mathrm{e}\lambda^2 r^2 \ln \frac{(\pi\mathrm{e})^{1/4}\lambda^{1/2} r}{2} - 2z^2 = E^2, \quad 0 \leqslant E^2 \leqslant \frac{2\lambda}{(\pi\mathrm{e})^{1/2}}. \tag{A7}$$

It is of some interest to examine the form of the secondary ovals in the limit as $E^2 \to 2\lambda/(\pi\mathrm{e})^{1/2}$. Firstly we note that for $E^2 = 2\lambda/(\pi\mathrm{e})^{1/2}$ the oval reduces to the single point $(r, z) = (2\pi^{-1/4}\,\mathrm{e}^{-3/4}\,\lambda^{-1/2}, 0)$. We then write

$$r = 2\pi^{-1/4}\,\mathrm{e}^{-3/4}\,\lambda^{-1/2} + \rho, \quad E^2 = 2\lambda/(\pi\mathrm{e})^{1/2} - \varepsilon^2. \tag{A8}$$

Expanding the first term on the LHS (A7) as a Taylor series in ρ about $r = 2\pi^{-1/4}\,\mathrm{e}^{-3/4}\,\lambda^{-1/2}$, we find

$$-\mathrm{e}\lambda^2 r^2 \ln \frac{(\pi\mathrm{e})^{1/4}\lambda^{1/2} r}{2} = \frac{2\lambda}{(\pi\mathrm{e})^{1/2}} - \mathrm{e}\lambda^2\rho^2 + \ldots. \tag{A9}$$

It follows that, in the limit as $E^2 \to 2\lambda/[(\pi\mathrm{e})^{1/2}]$, equation (A7) reduces to

$$\mathrm{e}\lambda^2\rho^2 + 2z^2 = \varepsilon^2 \tag{A10}$$

i.e. the logarithmic ovals reduce to ellipses with aspect ratio $\lambda(\mathrm{e}/2)^{1/2}$ centred on $(2\pi^{-1/4}\,\mathrm{e}^{-3/4}\,\lambda^{-1/2}, 0)$.

As E^2 increases from 0 to $2\lambda/(\pi\mathrm{e})^{1/2}$, the aspect ratio of the ovals increases from λ to $\lambda(\mathrm{e}/2)^{1/2}$ and their shape changes systematically from that of a primary logarithmic oval to that of an ellipse.

Curve 0 of Fig. 4 is a plot of the primary logarithmic oval, equation (A6). The curve labelled n ($n = 1, 2, \ldots, 10$) is a plot of the secondary logarithmic oval, equation (A7), for $E^2 = n\lambda/5(\pi\mathrm{e})^{1/2}$.

LA CONVECTION LIBRE A SYMETRIE AXIALE AUX PETITS NOMBRES DE RAYLEIGH DANS LES CAVITES POREUSES

Résumé—On trouve de différentes solutions précises pour la convection à symétrie axiale aux petits nombres de Rayleigh (R) provoquée par un gradient de température stationnaire et radial qui est perpendiculaire au champ de gravitation. On présente en détail des résultats pour des cavités cylindriques et toroïdales à rapport arbitraire des axes (λ). La valeur de R critique pour l'application de l'analyse est de $O(\lambda^{3/2})$ aux grandes valeurs de λ, de $O(1)$ pour $0{,}1 \leqslant \lambda \leqslant 1$, et aux petites valeurs de λ elle est de $O(\lambda^{-1/2})$ pour les toroïdes et de $O(\lambda^{-1/2}[-\ln\lambda]^{-1})$ pour les cylindres. Les solutions précises pour les toroïdes donnent un aperçu de la caractéristique de rouleau toroïdal de la convection à symétrie axiale aux petites valeurs de R.

Pour les cylindres (ainsi que pour la convection à deux dimensions aux petites valeurs de R dans le cas des rectangles) un écoulement de coeur avec des couches limites se produit et quand $\lambda \to 0$ et quand $\lambda \to \infty$. Le type d'écoulement dans les toroïdes (ainsi que dans les ellipses) est cependant invariant, sans écoulement de coeur ni couches limites.

De grandes analogies entre la convection à symétrie axiale et celle à deux dimensions aux petites valeurs de R valent également pour les propriétés telles que la variation avec λ de l'intensité de la convection et de la valeur critique de R.

DIE ACHSENSYMMETRISCHE FREIE KONVEKTION BEI KLEINER RAYLEIGH-ZAHL IN PORÖSEN HOHLRÄUMEN

Zusammenfassung—Verschiedene genaue Lösungen werden für achsensymmetrische Konvektion gefunden, die durch ein stationäres, radiales, zum Gravitationsfeld senkrechtes Temperaturgefälle in porösen Hohlräumen bei kleiner Rayleigh-Zahl (R) hervorgerufen ist. Ausführliche Ergebnisse werden für zylindrische sowie ringförmige Hohlräume mit beliebigem Achsenverhältnis (λ) angegeben. Der für die Anwendung der Analyse kritische R-Wert ist $O(\lambda^{3/2})$ bei grossen λ-Werten, $O(1)$ bei $0{,}1 \leqslant \lambda \leqslant 1$ und bei kleinen λ-Werten $O(\lambda^{-1/2})$ für Toroide und $O(\lambda^{-1/2}[-\ln \lambda]^{-1}$ für Zylinder. Die genauen Lösungen für Toroide geben Einsicht in die ringwulstige Charakteristik der achsensymmetrischen Konvektion bei kleinen R-Werten.

Für Zylinder (sowie für zweidimensionale Konvektion bei kleinen R-Werten in Rechtecken) findet eine Kernströmung mit Grenzschichten sowohl wenn $\lambda \to 0$ als auch wenn $\lambda \to \infty$ statt. Bei Toroiden (sowie bei Ellipsen) ist das Strömungsbild jedoch gleichbleibend, ohne Kerne noch Grenzschichten.

Gute Analogien zwischen achsensymmetrischer und zweidimensionaler Konvektion bei kleinen R-Werten gelten auch für solche Eigenschaften wie die Änderung mit λ der Konvektionsstärke sowie des kritischen R-Wertes.

СВОБОДНАЯ АКСИАЛЬНО-СИММЕТРИЧНАЯ КОНВЕКЦИЯ ПРИ НЕБОЛЬШИХ ЗНАЧЕНИЯХ ЧИСЛА РЕЛЕЯ ВНУТРИ ПОРИСТЫХ ПОЛОСТЕЙ

Аннотация — Различные точные решения получается для аксиально-симметричной конвекции внутри пористых полостей обусловена устойчивым радиальным температурным градиентом перпендикулярным к гравитационному полю. Подробные результаты представляются для цилиндрических и тороидальных полостей с произвольным соотношением длиной оси к короткой (λ). Критическое число Релея для применения анализа при больших значениях λ — $O(\lambda^{3/2})$, при $0{,}1 \leqslant \lambda \leqslant 1$ — $O(1)$ и при небольших значениях λ — $O(\lambda^{-1/2})$ для тороидов, а для цилиндров — $O(\lambda^{-1/2}[-\ln \lambda]^{-1})$. Точные решения для тороидов позволяют понимать особенность тороидального свертка аксиально-симметричной конвекции при небольших числая Релея.

Для цилиндров (и также для двухмерной конвекции при небольших значениях числа Релея внутри прямоугольников) ядровный поток с пограничными слоями существует, когда $\lambda \to 0$ и когда $\lambda \to \infty$. Однако, характер потока в тороидах (и также в эллипсах) — инвариантна, без ядер и пограничных слоев.

Близкие аналогии между аксиально-симметричной и двухмерной конвекции при небольших числах Релея существуют также для таких особенностей как изменение с сили конвекции и критического значения числа Релея.